



Full paper / Mémoire

## Investigations of the structure of the iron oxide semiconductor–electrolyte interface

Vladimir M. Aroutiounian<sup>a,\*</sup>, Valeri M. Arakelyan<sup>a</sup>, Gohar E. Shahnazaryan<sup>a</sup>,  
Gnel M. Stepanyan<sup>a</sup>, Emma A. Khachaturyan<sup>a</sup>, John A. Turner<sup>b</sup>

<sup>a</sup> Yerevan State University, 1 Alek Manoikian St., Yerevan 375025, Republic of Armenia

<sup>b</sup> National Renewable Energy Laboratory, Golden, 1617 Cole Boulevard, Golden, Colorado 80401-3393, USA

Received 19 August 2004; accepted after revision 17 March 2005

Available online 13 September 2005

### Abstract

The ceramic semiconductor photoelectrodes made of  $\text{Fe}_{1.99}\text{Sn}_{0.01}\text{O}_3$ ,  $\text{Fe}_{1.99}\text{Nb}_{0.01}\text{O}_3$ ,  $\text{Fe}_{1.8}\text{Nb}_{0.2}\text{O}_3$  and  $\text{FeNbO}_4$  are synthesized. The spectral and current–voltage characteristics of photoelectrodes are measured. The anodic photocurrent onset potential is determined. The threshold photon energies corresponding to the inter-band optical transitions near the edge of the fundamental absorption of the semiconductor photoelectrode are calculated. The analysis of the frequency dispersion of the real and imaginary parts of the complex impedance of photoelectrochemical cell with manufactured electrodes is carried out. On the basis of this analysis, equivalent circuits describing the structure of the double electrical layer on the semiconductor–electrolyte interface are proposed, their parameters are calculated. Main limiting steps of the electrode process are determined. **To cite this article:** *V.M. Aroutiounian et al., C. R. Chimie 9 (2006).*

© 2005 Académie des sciences. Published by Elsevier SAS. All rights reserved.

### Résumé

Des céramiques de  $\text{Fe}_{1.99}\text{Sn}_{0.01}\text{O}_3$ ,  $\text{Fe}_{1.99}\text{Nb}_{0.01}\text{O}_3$ ,  $\text{Fe}_{1.8}\text{Nb}_{0.2}\text{O}_3$  et  $\text{FeNbO}_4$  ont été synthétisées pour être utilisées comme photoélectrodes. Les caractéristiques courant–tension et les réponses spectrales de ces photoélectrodes et le potentiel de début du photocourant anodique ont été mesurés. Le seuil d'absorption d'énergie des photons correspondant aux transitions optiques inter-bandes des semiconducteurs a été calculé. L'analyse de la fréquence de dispersion des parties réelles et imaginaires des impédances complexes des cellules photoélectrochimiques fabriquées à partir de ces photoélectrodes a été effectuée. Sur la base de cette analyse, des circuits équivalents décrivant la structure de la double couche électrique de l'interface semiconducteur–électrolyte ont été proposés et leurs paramètres calculés. Les étapes limitantes du processus d'électrode ont été déterminées. **Pour citer cet article :** *V.M. Aroutiounian et al., C. R. Chimie 9 (2006).*

© 2005 Académie des sciences. Published by Elsevier SAS. All rights reserved.

**Keywords:** Iron oxide; Ceramic photoelectrode; Interface; Impedance; Equivalent circuits

**Mots-clés :** Oxyde de fer ; Photoélectrode céramique ; Impédance ; Circuits équivalents

\* Corresponding author.

E-mail addresses: [kisahar@ysu.am](mailto:kisahar@ysu.am) (V.M. Aroutiounian), [jturner@nrel.gov](mailto:jturner@nrel.gov) (J.A. Turner).

## 1. Introduction

Today metal-oxide semiconductors are the most promising materials for photoelectrochemical conversion of solar energy by the photoelectrolysis of water since the problem of the stability of photoelectrodes are basically solved only for such materials [1–4]. The efficiency of the processes that take place in photoelectrochemical cells is determined by the crystalline structure, bulk and surface properties of semiconductor photoelectrode, its corrosion resistance in aqueous electrolytes and ability to drive the water-splitting reaction, as well as by the structure and properties of the semiconductor–electrolyte interface. Such an interface is a rather complicated system, and despite numerous studies, it is not yet fully understood. Investigations of such two-phase interface properties and physical-chemical processes taking place at the interface play an important role both for fundamental analysis of these processes and in our understanding of the rather low efficiency for hydrogen production and to determine ways to improve the efficiency of photoelectrochemical conversion of solar energy up to the theoretically possible maximal values. Therefore, from this viewpoint, investigations of properties and structure of the two-phase interface by the method of the electrochemical impedance spectroscopy are very promising and informative [5–7].

Note that this method measures of the frequency dependences of the real and imaginary components of the complex impedance of the electrochemical cell. The analysis of these characteristics provides information about the structure of the electrical double layer at the semiconductor–electrolyte interface and the charge transfer processes in the semiconductor and electrolyte, as well as allowing to calculate parameters determining the limiting steps of the electrode processes.

The aim of this paper is the investigations of the metal oxide semiconductor–electrolyte interface structure using the technique of the impedance spectroscopy. We used as photoelectrodes, fabricated by us, polycrystalline samples of  $\text{Fe}_{1.99}\text{Sn}_{0.01}\text{O}_3$ ,  $\text{Fe}_{1.99}\text{Nb}_{0.01}\text{O}_3$ ,  $\text{Fe}_{1.8}\text{Nb}_{0.2}\text{O}_3$ , and  $\text{FeNbO}_4$ .

## 2. Experimental

Rhombohedral iron oxide (hematite,  $\alpha\text{-Fe}_2\text{O}_3$ ) was chosen as the starting material for manufacturing these

polycrystalline photoelectrodes. Iron oxide ( $\text{Fe}_2\text{O}_3$ ) is an insulator with specific electroconductivity of  $\sim 10^{-12} \Omega^{-1} \text{cm}^{-1}$  at room temperature. The semiconductor phases are prepared by the doping of  $\text{Fe}_2\text{O}_3$  with transition metal ions ( $\text{Sn}^{4+}$  or  $\text{Nb}^{5+}$ ). It is known that the levels of these ions are located above the level of iron ions [8]. Therefore, their introduction into the  $\text{Fe}_2\text{O}_3$  lattice results in the change in part of  $\text{Fe}^{3+}$  ions to bivalent state. The existence in equivalent points of the lattice of the same element ions with different valences ( $\text{Fe}^{2+}$  and  $\text{Fe}^{3+}$ ) leads to the hopping mechanism of the conductivity. This is associated with electron exchange via thermal excitation between these ions.

For solid-phase reaction the corresponding amounts of starting oxides ( $\text{Fe}_2\text{O}_3$ ,  $\text{Nb}_2\text{O}_5$ ,  $\text{SnO}_2$ ) were mixed in high purity ethanol. After preliminary sintering in the air at 900 °C for 7 h the mixed powders were pressed into compact pellets. These pellets were then again sintered in air at temperatures of 1250–1300 °C. The time of synthesis was  $\sim 10$  and 15 h for doping with Sn and Nb, respectively. The homogeneity of the sintered phases was measured by X-ray phase analysis. The results of these measurements showed that synthesized samples with concentrations of tin or niobium of 0.5 atomic percent are homogeneous and completely keep the iron oxide (hematite) structure, i.e. full dissolution of the doping element and the formation of a substitution solid solution takes place. The doped samples  $\text{Fe}_{1.99}\text{Sn}_{0.01}\text{O}_3$  and  $\text{Fe}_{1.99}\text{Nb}_{0.01}\text{O}_3$  were n-type and had specific electroconductivity of  $\sim 10^{-2} \Omega^{-1} \text{cm}^{-1}$ . The investigations of the temperature dependencies of the electroconductivity in the range of 77–500 K established that donor centers with an ionization energy of  $\sim 0.3\text{--}0.4$  eV are formed by doping. The connecting of local pairs  $\text{Fe}^{+2}\text{--M}^{+n}$  with electrostatic forces played the role of donor centers in these compositions.

The solid solutions  $\text{Fe}_{1.8}\text{Nb}_{0.2}\text{O}_3$  and  $\text{FeNbO}_4$  were also synthesized by solid-phase reactions. For the synthesis of the solid solutions, consistent with the above approach, the same attempt to combine the best characteristics of each material is made: the good spectral characteristics of photoelectrodes  $\text{Fe}_2\text{O}_3$  and the rather negative flat-band potential of  $\text{Nb}_2\text{O}_5$  photoelectrodes. The initial ratios of components were taken to provide compositions of  $\text{Fe}_{1.8}\text{Nb}_{0.2}\text{O}_3$  ( $\text{Fe}_2\text{O}_3 + 10$  at. % Nb) and  $\text{FeNbO}_4$  ( $\text{Fe}_2\text{O}_3 + 50$  at. % Nb). After preliminary sintering in the air at 1000 °C for 5 h and thorough mixing in agate mortar, the compact pellets were then

again sintered in air at temperatures of 1250 °C continuously during 24 h. We obtained a two-phase material at 10 at. % Nb. In the X-ray pattern all lines relating to  $\alpha$ -Fe<sub>2</sub>O<sub>3</sub> are present along with two additional lines relating to the FeNbO<sub>4</sub> phase. The composition with 50 at. % Nb is phase homogeneous with the FeNbO<sub>4</sub> structure. Additional lines connected with other phases are not observed in the X-ray pattern. The synthesized solid solutions Fe<sub>1.8</sub>Nb<sub>0.2</sub>O<sub>3</sub> and FeNbO<sub>4</sub> had specific electroconductivity of  $\sim 10^{-3} \Omega^{-1} \text{ cm}^{-1}$ .

Photoelectrodes were prepared from the synthesized ceramics. Pellets were cut from the wafers with a thickness of  $\sim 1 \text{ mm}$  and an area of  $\sim 0.25 \text{ cm}^2$ . Ohmic contacts were made by vacuum deposition of copper. An electric lead was soldered to the copper and covered with an epoxy adhesive.

The spectral characteristics of photoelectrodes were obtained by the measurement of the photoreponse from the ceramic photoelectrode placed in a homogeneous photoelectrochemical cell. The photoelectrode was illuminated with light from a high-pressure 1-kW xenon-lamp passing through a monochromator. The photoreponse was recorded on the recording instrument KSP-4. The investigation of the current–voltage characteristics of the photoelectrodes was carried out in the same photoelectrochemical cell.

Measurements of the frequency dependencies of the real and imaginary parts of the complex impedance of the electrochemical cell with the synthesized electrodes were carried out using a Solartron 1287 EI potentiostat and the 1260 FRA frequency response analyzer in conventional cell with a platinum counter-electrode and a saturated calomel reference electrode (SCE) in the dark. Investigations were carried out in 5 N NaOH aqueous electrolyte at different electrode potentials with a.c. amplitude of 7 mV. The frequency was varied between 0.1 and  $3 \times 10^5 \text{ Hz}$ .

The investigation of the photoelectrolysis current was carried out using from a 200-W mercury-lamp. The compartments of the photoelectrochemical cell were

separated by the MF-4SK ion-exchanging membranes and filled with aqueous 5 N NaOH (anode) and 5 N H<sub>2</sub>SO<sub>4</sub> (cathode) electrolyte, respectively. Platinum was used as counter-electrode.

### 3. Results and discussion

We used polycrystalline samples of Fe<sub>1.99</sub>Sn<sub>0.01</sub>O<sub>3</sub>, Fe<sub>1.99</sub>Nb<sub>0.01</sub>O<sub>3</sub>, Fe<sub>1.8</sub>Nb<sub>0.2</sub>O<sub>3</sub>, and FeNbO<sub>4</sub> as semiconductor photoanodes. The photoelectrochemical characteristics of the photoelectrodes were investigated. The region of spectral photosensitivity for the electrodes made of solid solutions coincides with the region of spectral photosensitivity for doped photoelectrodes and covers the wavelengths spectrum from 270 to 670 nm. The peak sensitivity of photoelectrode FeNbO<sub>4</sub> corresponds to  $\sim 390 \text{ nm}$  (for doped photoelectrodes the photocurrent peak is between  $\sim 430$  and  $490 \text{ nm}$ ). Investigations of the inter-band phototransitions in the semiconductor near the fundamental absorption edge established that the main contribution to the photocurrent of doped photoelectrodes is given by two optical transitions with energies  $\sim 1.83$  and  $2.45 \text{ eV}$ . Most probably, the first transition corresponds to the excitation of charge carriers between  $d \rightarrow d$  states of iron ions, and second transition corresponds to the excitation between 2 p states of oxygen and 3 d states of iron. A hole is formed in the iron d states in the first case and in the oxygen valence band in the second case. The photocurrent for the FeNbO<sub>4</sub> electrodes is also characterized by two indirect optical transitions. The threshold photon energies corresponding to these transitions are  $\sim 2$  and  $2.66 \text{ eV}$ .

The anodic photocurrent onset potential ( $\varphi$ ) of the photoelectrodes was determined from measurements of the current–voltage characteristics of photoelectrodes (Table 1). A noticeable shift of the flat-band potential to the negative direction took place for the FeNbO<sub>4</sub> photoelectrodes; the photocurrent onset was observed at a more negative external bias.

Table 1  
Photocurrent and parameters of the high-frequency equivalent electrical circuit

Electrodes composition	$\varphi, \text{ V}$	$I_{\text{ph}}, \text{ mA cm}^{-2}$ homogeneous cell, $U_{\text{bias}} = 0.6 \text{ V}$	$I_{\text{ph}}, \text{ mA cm}^{-2}$ heterogeneous cell	$R_0, \Omega$	$C_1 \times 10^{-8}, \text{ F}$	$R_1, \Omega$
Fe <sub>1.99</sub> Sn <sub>0.01</sub> O <sub>3</sub>	-0.33	0.18	0.24	45	4.57	310
Fe <sub>1.99</sub> Nb <sub>0.01</sub> O <sub>3</sub>	-0.25	0.21	0.28	100	4.61	11060
Fe <sub>1.8</sub> Nb <sub>0.2</sub> O <sub>3</sub>	-0.35	0.35	0.41	80	7.04	4140
FeNbO <sub>4</sub>	-0.55	0.56	0.6	230	3.12	7280

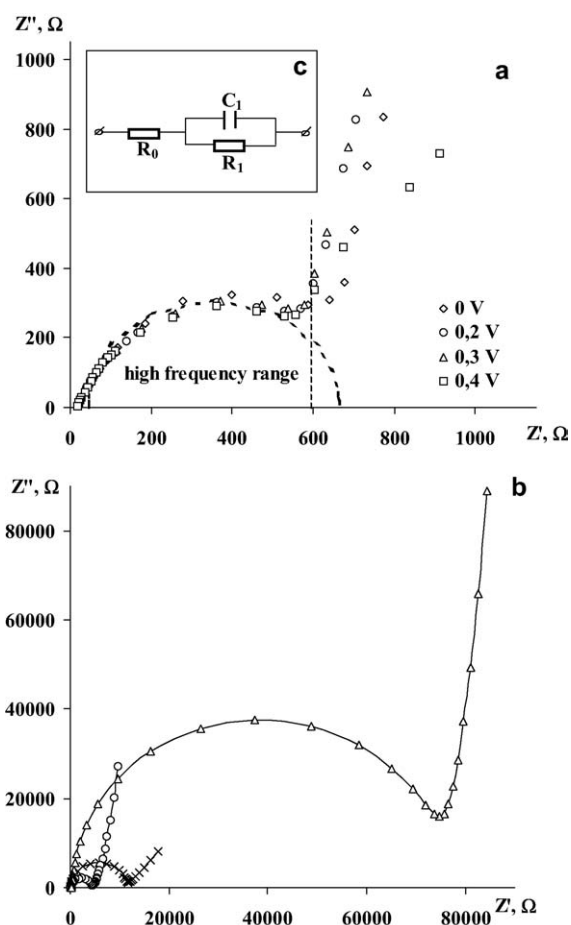


Fig. 1. The Nyquist plots for the electrode  $\text{Fe}_{1.99}\text{Sn}_{0.01}\text{O}_3$  at different electrode potentials (a),  $\text{Fe}_{1.99}\text{Nb}_{0.01}\text{O}_3$  ( $\times$ ),  $\text{Fe}_{1.8}\text{Nb}_{0.2}\text{O}_3$  ( $\circ$ ) and  $\text{FeNbO}_4$  ( $\Delta$ ) at the electrode potential 0 V vs. SCE (b); the equivalent circuit used for the modeling of the electrochemical cell in high frequency range (c).

As mentioned above, the measurements of frequency dependencies of the real ( $Z'$ ) and imaginary ( $Z''$ ) parts of the complex impedance of the electrochemical cell with the synthesized electrodes were carried out to investigate of the structure of the semiconductor–electrolyte interface. Some results of our measurements are presented in Fig. 1 in the form of the Nyquist plots.

For the analysis of the frequency dependence of the impedance, the simulation method of the electrochemical cells was used where the response of the cell is modeled by an equivalent circuit, which has a response to the external signal identical to the response of the electrochemical cell. Two possible approaches can be found

in the literature. According to the first, an equivalent circuit comprising a capacitance, which simulates the semiconductor–electrolyte interfaces, and a resistance connected in parallel. The potential dependences of these elements are then calculated. The second approach involves a more complicated equivalent circuit for the electrochemical cell; however, the elements of this circuit are frequency independent. Both approaches have their advantages and disadvantages. In the first case, for example, difficulties in finding an adequate theoretical explanation for the frequency dependences were observed. In the second case, the difficulties lie in finding an equivalent circuit whose impedance is the closest to the one measured experimentally [9–13].

We follow the first methodology in our investigations. According to the generally accepted model, three ranges are selected in the frame of a double electrical layer formed on the semiconductor–electrolyte interface: the space-charge layer of the semiconductor; the diffuse ionic layer of the electrolyte (the Gouy layer); and the intermediate Helmholtz layer corresponding to one or two atomic layers. Therefore, the differential capacity of the semiconductor–electrolyte interface represents three capacities connected in series: the capacity of the space-charge layer of the semiconductor, the capacity of the Gouy layer and capacity of the Helmholtz layer. Practically, the main part of an interface potential occurs as an overall voltage drop in the space-charge layer of the semiconductor and as a result, the main contribution to their capacity comes from the capacity of the space-charge layer in the semiconductor. Therefore, for the elementary case, the equivalent electrical circuit of the electrochemical cell (Fig. 1c) consists of a resistance  $R_0$ , characterizing the series-connected resistances of the electrolyte and the semiconductor's bulk, the capacitor,  $C_1$ , appropriate capacity of the semiconductor's space-charge layer, and the resistance,  $R_1$ , describing a stage of discharge–transport of charge carriers through the interface. The real and imaginary components of the complex impedance for such a circuit are calculated according to the formulas:

$$Z' = R_0 + \frac{R_1}{1 + \omega^2 R_1^2 C_1^2} \quad \text{and} \quad Z'' = \frac{\omega R_1^2 C_1}{1 + \omega^2 R_1^2 C_1^2} \quad (1)$$

and the Nyquist plot has the form of a semicircle. The results of our measurements, both for doped

photoelectrodes  $\text{Fe}_2\text{O}_3$  and for solid solutions from  $\text{Fe}_2\text{O}_3\text{-Nb}_2\text{O}_5$  system show that two ranges of frequencies are observed in the frequency characteristics in all cases. The Nyquist semicircle in the high frequency range shows that the contribution to the impedance of the electrochemical cells is determined by the space-charge layer for investigated semiconductor electrodes. The results of these measurements of the complex impedance of the electrochemical cells allows the isolation of capacity  $C_1$ , and also the calculation of other parameters of the high-frequency equivalent electrical circuit. The value  $R_0$  corresponds to the left edge of the Nyquist semicircle. The imaginary part of the complex impedance has a maximum, which is equal to  $R_1/2$ . From the condition  $R_1 C_1 \omega^{\max} = 1$ , the semiconductor's space-charge layer capacitance,  $C_1$ , was determined. Results of calculations for the measurements of an impedance carried out at 0 V vs. SCE are indicated in Table 1.

The majority of experimental impedance characteristics deviate from Eq. (1) at low frequencies. Such impedance characteristics testify that the signals in the external circuit do not only reflect properties of investigated semiconductor electrode. The simple circuit (Fig. 1c) is inadequate and should be supplemented with elements taking into account other factors, which influence the photoelectrolysis process. For example, often an RC circuit is added to the equivalent electrical circuit, take into account the effect of surface levels and the Helmholtz layer, as well as non-uniformity of doping, generation-recombination processes, etc.

To define the equivalent electrical circuit needed for the modeling of the behavior of the electrochemical cell in the low frequency range, the vectorial subtraction of the impedance of the circuit presented in Fig. 1c from the whole impedance is carried out. For electrodes made of solid solutions  $\text{Fe}_{1.8}\text{Nb}_{0.2}\text{O}_3$  and  $\text{FeNbO}_4$ , the dependencies on frequency of the real component of the impedance remaining after vectorial subtraction ( $Z_1'$ ) are proportional to  $d/\omega^{1/2}$ . This dependence is typical for the Warburg impedance, which is connected with a slow diffusion processes. The values of the Warburg constant,  $d$ , was calculated from the slope of the straight line  $Z_1' = f(1/\omega^{1/2})$ . The frequency dependency of the imaginary component ( $Z_2''$ ) remaining after a second vectorial subtraction has a capacitive character. The value of the capacitance  $C_0$  was calculated from the

slope of the straight lines  $Z_2'' = f(1/\omega)$ . Thus, the electrochemical cell with the electrodes  $\text{Fe}_{1.8}\text{Nb}_{0.2}\text{O}_3$  or  $\text{FeNbO}_4$  is modeled by the equivalent electrical circuit represented in Fig. 2a at electrode potentials between 0 and 0.2 V vs. SCE. The physical meaning of the parameters  $R_0$ ,  $R_1$ ,  $C_1$  are mentioned above. The  $R_w C_w$  circuit corresponds to the Warburg diffusion impedance, and the capacity  $C_0$  is most probably connected with the presence of the Helmholtz layer. In this case, the main limiting steps of the electrode processes, which determine the electrode polarization and current, are the diffusion impedance and the large capacity connected with the presence of the Helmholtz layer.

Similar analysis of the real and imaginary components of impedance has allowed the development of the equivalent electrical circuit, presented in Fig. 3a for electrodes made of doped  $\text{Fe}_2\text{O}_3$ . The appearance in the low frequency range of the frequency dependent resistance for the semiconductor's bulk,  $R = a/\omega$ , is stipulated by the dispersion of conductivity, which is typical for oxides like  $\text{Fe}_2\text{O}_3$  with the hopping mecha-

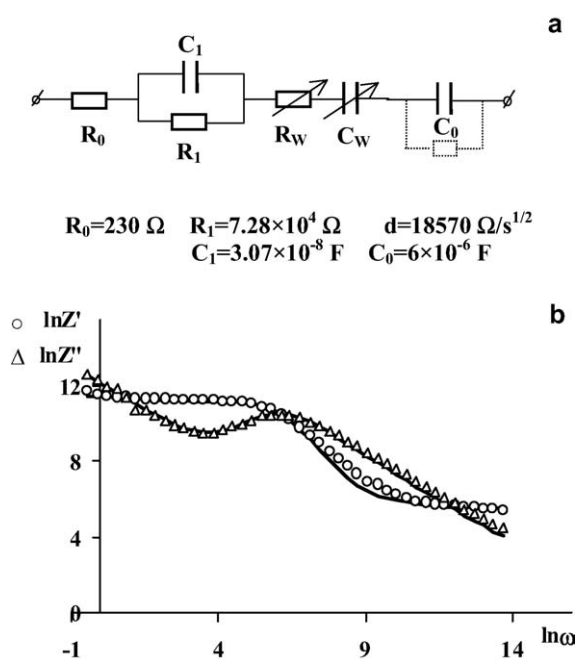


Fig. 2. (a) The equivalent circuit used for the modeling of the electrochemical cell with the electrode  $\text{FeNbO}_4$  at the electrode potential 0.2 V vs. SCE. (b) Frequency dependencies for the real and imaginary components of the complex impedance of the electrochemical cell with the electrode  $\text{FeNbO}_4$  at an electrode potential of 0.2 V vs. SCE. Points are experimental data. Solid lines are fits to the theoretical curves calculated for the equivalent circuit shown in (a).

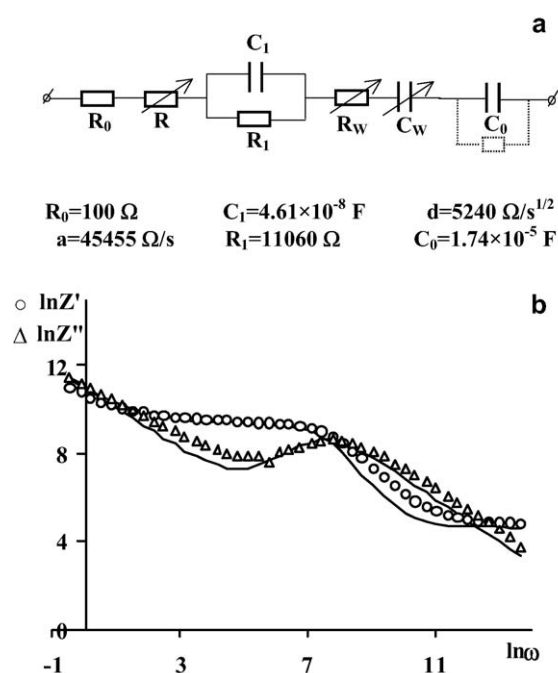


Fig. 3. (a) The equivalent circuit used for the modeling of the electrochemical cell with the electrode  $\text{Fe}_{1.99}\text{Nb}_{0.01}\text{O}_3$  at the electrode potential 0.2 V vs. SCE. (b) Frequency dependencies for the real and imaginary components of the complex impedance of the electrochemical cell with the electrode  $\text{Fe}_{1.99}\text{Nb}_{0.01}\text{O}_3$  at an electrode potential of 0.2 V vs. SCE. Points are experimental data. Solid lines are fits to the theoretical curves calculated for the equivalent circuit shown in (a).

nism for the electroconductivity. The equivalent electrical circuits proposed for the electrochemical cell with doped  $\text{Fe}_{1.99}\text{Sn}_{0.01}\text{O}_3$  and  $\text{Fe}_{1.99}\text{Nb}_{0.01}\text{O}_3$  electrodes indicate that the resistance of the semiconductor's bulk, the capacity connected with the Helmholtz layer, and slow diffusion supply of carriers to the electrode surface play a determining role for the electrode processes at the semiconductor–electrolyte interface. Results of the calculations of real and imaginary parts of the complex impedance for the proposed equivalent electrical circuit using obtained parameters of its components show the good fit of the calculations with the experimental data (Fig. 2b and Fig. 3b). Calculations of real and imaginary components were carried out according to the standard expressions given in [12].

Changes in the frequency dependencies of the impedance takes place with an increase in the electrode potential. The Nyquist plot consists of two semi-circles, pointing to a model of the electrochemical cell

with an equivalent circuit consisting of two series-connected RC circuits (Fig. 4). One of them,  $R_1C_1$ , characterizes the semiconductor's space-charge layer and contributes to the impedance in the high frequency range. The other circuit,  $R_2C_2$ , is most likely connected with the surface states, and the contribution of such circuit is exhibited in the low frequency range. Therefore, at electrode potentials more positive than 0.4 V vs. SCE, the process of the charging of surface levels in the low frequency range play determining role for the electrode processes at the semiconductor–electrolyte interface. It is confirmed by investigations of the dependence on applied external bias, which have shown that applied voltage is distributed between the semiconductor's space-charge layer and electrolyte and the change in the voltage drop in the semiconductor's space-charge layer is comparable with the voltage drop on the Helmholtz layer. The latter testifies to the presence of a high density of surface levels, the charge of which changes in the region of potentials investigated.

The results of the photocurrents measurements ( $I_{\text{ph}}$ ) are given in the Table 1. Photoelectrolysis takes place most efficiently with an external bias of 0.6 V in an aqueous solution of 5 N NaOH. The same was observed in a photoelectrochemical cell, when the anode and cathode compartments were filled with aqueous 5 N NaOH and 5 N  $\text{H}_2\text{SO}_4$  electrolyte, respectively (difference pH = 13). The displacement of the flat-band potential to negative energies and the elimination also of limiting step, connecting the frequency dependence of the

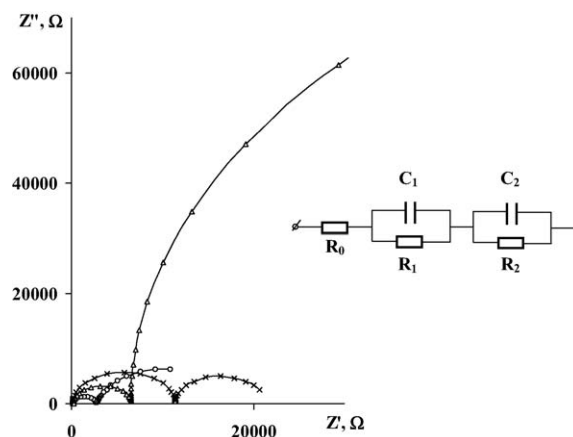


Fig. 4. The Nyquist plots for the electrodes  $\text{Fe}_{1.99}\text{Nb}_{0.01}\text{O}_3$  ( $\times$ ),  $\text{Fe}_{1.8}\text{Nb}_{0.2}\text{O}_3$  ( $\circ$ ) and  $\text{FeNbO}_4$  ( $\Delta$ ) at the electrode potential 0.6 V vs. SCE and the equivalent circuit used for the modeling of the electrochemical cell at large electrode potentials.

semiconductor's bulk resistance (the influence of this limitation is appreciable in the low frequency range  $\omega \rightarrow 0$ ) lead to the expected increase in the photocurrent by a factor of two for photoelectrodes made of solid solutions  $\text{Fe}_{1.8}\text{Nb}_{0.2}\text{O}_3$  and  $\text{FeNbO}_4$ . The rate of hydrogen evolution is  $\sim 15.3$  and  $22.4 \mu\text{mole h}^{-1} \text{cm}^{-2}$  for  $\text{Fe}_{1.8}\text{Nb}_{0.2}\text{O}_3$  and  $\text{FeNbO}_4$  photoelectrodes, respectively, at a difference  $\text{pH} = 13$  between anode and cathode compartments of photoelectrochemical cell and under illumination by the 200-W mercury lamp.

#### 4. Conclusion

Ceramic semiconductor photoelectrodes made up of n-type  $\text{Fe}_2\text{O}_3$  doped with 0.5 at.% Sn or Nb and solid solutions  $\text{Fe}_{1.8}\text{Nb}_{0.2}\text{O}_3$  and  $\text{FeNbO}_4$  were synthesized. The electrophysical and photoelectrochemical characteristics of these photoelectrodes were investigated.

The structure of two-phase interface was studied using impedance spectroscopy. On the basis of the analysis of the frequency dispersion of the real and imaginary parts of the complex impedance, the equivalent circuit for the description of the structure of the double electrical layer on the semiconductor–electrolyte interface are proposed, its corresponding parameters were calculated and the limiting steps of the electrode process were determined.

For the  $\text{Fe}_{1.99}\text{Sn}_{0.01}\text{O}_3$  and  $\text{Fe}_{1.99}\text{Nb}_{0.01}\text{O}_3$  photoelectrodes, the dispersion of conductivity, slow diffusion of charge carriers to the electrode surface and large capacitance of the Helmholtz layer are the main limiting factors for the electrode processes. For the  $\text{Fe}_{1.8}\text{Nb}_{0.2}\text{O}_3$ , and  $\text{FeNbO}_4$  photoelectrodes, two limiting stages were established: the Warburg diffusion impedance and re-charged Helmholtz layer.

The displacement of the flat-band potential to negative energies and removal of the limiting step linked to the dispersion of the semiconductor's bulk conductivity led to the increase in the photocurrent by a factor of

two for photoelectrodes made of solid solutions  $\text{FeNbO}_4$ , in comparison with photoelectrodes made up of doped  $\text{Fe}_2\text{O}_3$ .

#### Acknowledgements

These investigations were carried out in the framework of the ISTC A-322 grant and ANSEF grant N 04-PS-cheminorg-728-25.

#### References

- [1] V.M. Aroutiounian, in: K.I. Zamaraev, V.N. Parmon (Eds.), Photocatalytic Conversion of Solar Energy, Nauka, Novosibirsk, 1991, p. 228 (in Russian).
- [2] A.G. Sarkissyan, J. Contemp. Phys. 30 (1995) 21.
- [3] V.M. Aroutiounian, in: P. Catania, B. Golchert, C.Q. Zhou (Eds.), Energex 2000: Proc. 8th Intern. Energy Forum, Balaban Publ., Las Vegas, 2000, p. 318.
- [4] V.M. Aroutiounian, V.M. Arakelyan, G.E. Shahnazaryan, in: S.A. Rahman, K. Sopian, A.Z. Ahmed, M.Y. Othman (Eds.), Environment Protection and Energy Solution for Sustainable Development, Kuala Lumpur, Malaysia, 2003, p. 171.
- [5] S.S. Kocha, J.A. Turner, Electrochim. Acta 41 (1996) 1295.
- [6] V.M. Aroutiounian, V.M. Arakelyan, G.E. Shahnazaryan, G.M. Stepanyan, J.A. Turner, S.S. Kosha, in: J.C. Bolcich, T.N. Veziroglu (Eds.), Proc. 12th World Hydrogen Energy Conf., Buenos Aires, Argentina, 1998, vol. 3, p. 2149.
- [7] V.M. Aroutiounian, V.M. Arakelyan, G.E. Shahnazaryan, G.M. Stepanyan, J.A. Turner, Russ. J. Electrochem. 35 (1999) 854.
- [8] S. Krupicka, in: Physik der Ferrite und der verwandten magnetischen Oxide, vol. 2, Academia, Prague, 1973. Translated under the title Fizika ferritov i rodstvennykh im magnitnykh okislov, vol. 2, Mir, Moscow, 1976, p. 435.
- [9] J. Schefold, J. Electrochem. Soc. 142 (1995) 850.
- [10] J. Schefold, J. Electrochem. Soc. 143 (1996) 1598.
- [11] A.G. Sarkissyan, G.E. Shahnazaryan, V.M. Arakelyan, V.M. Aroutiounian, K.H. Begoyan, Russ. J. Electrochem. 33 (1997) 753.
- [12] V.M. Aroutiounian, V.M. Arakelyan, G.E. Shahnazaryan, G.M. Stepanyan, J.A. Turner, S.S. Kosha, Electrochim. Acta 45 (2000) 1999.
- [13] V.M. Aroutiounian, V.M. Arakelyan, G.E. Shahnazaryan, G.M. Stepanyan, J.A. Turner, O. Khaselev, Russ. J. Electrochem. 38 (2002) 378.